# Parameterization of Turbulent and Mesoscale Fluxes for Heterogeneous Surfaces

ANTTI AROLA

*Department of Meteorology, University of Helsinki, Helsinki, Finland*

(Manuscript received 14 April 1997, in final form 10 April 1998)

ABSTRACT

Improved parameterizations for turbulent surface fluxes over inhomogeneous terrain at several scales of heterogeneity are developed, and mesoscale numerical model results are used to evaluate them. The extension to the mosaic method, which uses stability corrected logarithmic profiles to calculate local wind speed, air temperature, and specific humidity estimates at the reference level over each surface cover, gave promising results for the larger scales of surface heterogeneity. A simple temperature adjustment method is also proposed as an extension to the basic mosaic method. At smaller scales of heterogeneity, it was shown that further improvements for the parameterization of momentum transfer are needed. These are likely to be carried out by introducing mechanisms to incorporate the effects of form drag in conjunction with the ''three-resistance'' model.

Based on similarity theory, simple parameterization schemes for the mesoscale heat fluxes are proposed. The parameterizations are validated with several surface and atmospheric conditions, and they turn out to be quite robust.

## 1. Introduction

General circulation models (GCMs) used for climate simulation and weather prediction require parameterizations for many unresolved processes at the computational grid scale. Within the typical GCM grid size of 200–800-km, strong landscape heterogeneities usually exist. In recent years there has been increasing research interest in the treatment of subgrid-scale heterogeneities in atmospheric models. Mahrt (1987) pointed out some problems on grid-flux estimates caused by the subgrid-scale heterogeneity. One approach to resolving these problems was suggested by Avissar and Chen (1993). In their approach, the large-scale (model grid box) averaged vertical flux is decomposed, at any height, assuming scale separation between the mesoscale and turbulent contribution,

$$\langle w\phi\rangle = \langle w'\phi'\rangle + \langle w''\phi''\rangle, \tag{1}$$

where $\phi$ represents quantities such as temperature, specific humidity, or one of the velocity components; $w$ represents vertical velocity; and $\langle\ \rangle$ stands for area average. The first term on the right-hand side of the decomposition represents the contribution of mesoscale circulations (if any) and the second term represents contributions from small-scale turbulent motion, which is superimposed on the mesoscale perturbation. The mesoscale flux contribution, with the exception of gravity wave drag, is neglected in current GCMs. Only very recently has there been research directed at parameterization of other systematic mesoscale effects (Lynn et al. 1995; Zeng and Pielke 1995; Savijärvi 1995). Most of the current generation of GCMs use turbulent transfer schemes, which are based on experiments over homogeneous surfaces (e.g., Businger et al. 1971), so they may not be valid for heterogeneous surfaces. In other words, in both contributions in the above decomposition, there is room for improvement.

Some current GCM land surface parameterizations (LSPs) have begun to use the mosaic method for turbulent surface fluxes over heterogeneous terrain (Avissar and Pielke 1989; Koster and Suarez 1992; Ducoudré et al. 1993). In the mosaic method the surface grid square is divided into homogeneous subareas (''tiles,'' ''patches'') that interact independently with the overlying atmosphere. The effects of local horizontal advection are thus assumed unimportant when compared to the magnitudes of the local vertical fluxes.

For sensible heat flux $H$, for example, the basic mosaic method can be expressed as

$$\langle H\rangle = \sum_{i=1}^{n} \rho c_p f_i C_H^i \langle V_z\rangle(\theta_s^i - \langle\theta_z\rangle), \tag{2}$$

where $n$ is the number of patches in the GCM grid, $f_i$ is the fraction of the grid area covered by the patch $i$, $\rho$ is the air density, $c_p$ is the specific heat, $C_H^i$ is the transfer coefficient for the surface type $i$, and $\theta_s$ is the

*Corresponding author address:* Antti Arola, Finnish Meteorological Institute, P.O. Box 503 (Vuorikatu 19), FIN-00101 Helsinki, Finland.
E-mail: antti.arola@fmi.fi

surface potential temperature. Here $\langle V_z \rangle$ and $\langle \theta_z \rangle$ are the area-averaged wind speed and potential temperature at the reference level, which is usually the lowest GCM level. The concept of blending height (e.g., Wieringa 1986; Mason 1988; Wood and Mason 1991) has been proposed to incorporate the horizontal advection effects of heterogeneity on the surface turbulent fluxes. The method proposed by Blyth (1995) combines these approaches into a scale-dependent resistance configuration, which she called the three-resistance model. A statistical–dynamical approach has also been suggested for the parameterization of turbulent surface fluxes in GCMs (Avissar 1992). In this approach probability density functions are used to represent the spatial variability of particular variables.

Current LSP schemes can thus account for inhomogeneous surface properties to some extent. However, they normally neglect the effects of associated variability in the boundary layer characteristics. For instance, the basic mosaic method assumes spatially homogeneous near-surface atmospheric conditions. Doran and Zhong (1995) found, within an area comparable to the size of a GCM grid square, substantial differences (about 30%) in the grid-average sensible heat flux computed with mesoscale model-produced local values of wind speed and air temperature, as compared to those computed with spatial averages of wind speed and air temperature, $\langle V_z \rangle$ and $\langle \theta_z \rangle$ (i.e., as in most current GCM schemes).

The reference level is typically the lowest atmospheric model level. However, over heterogeneous surfaces the lower parts of the boundary layer are heterogeneous as well, and two main problems with the use of the mosaic method can be distinguished. First, at large scales of heterogeneity (typically $>$10 km), wind speed, air temperature, and specific humidity can vary significantly at the lowest model level and in turn the use of grid-area-averaged values in the mosaic method cannot predict the area average flux correctly. Secondly, at smaller scales of heterogeneity, while wind speed, air temperature, and specific humidity now may be homogeneous at the lowest model level, the horizontal advection effects near the surface can be significant and the basic mosaic method fails to predict area-averaged surface fluxes.

Equation (1) expressed the total area-mean vertical subgrid-scale fluxes within the GCM grid element. It is stressed that current parameterizations for turbulent fluxes for heterogeneous surfaces require improvements and that at the middle and upper part of the boundary layer the mesoscale fluxes may sometimes be larger in magnitude than the turbulent fluxes (e.g., Pielke et al. 1991). However, there has been only little effort toward developing parameterizations for mesoscale fluxes. The main goal of our study therefore is to seek for improvements for both the turbulent surface flux and the mesoscale flux parameterizations for current GCMs. In the study presented in this paper extensions of the basic mosaic method are developed and tested for parameterization of turbulent surface fluxes for heterogeneous surfaces at different spatial scales. Furthermore, parameterizations for the mesoscale sensible and latent heat fluxes are developed.

## 2. Approach

The mesoscale model of the University of Helsinki is used to represent a single GCM grid box under steady-state large-scale conditions—that is, assuming a steady large-scale pressure gradient in the form of a background geostrophic wind. The approach allows investigation of interactions of the subgrid-scale surface and atmospheric processes and estimation of grid-averaged fluxes of both the turbulent and the mesoscale flux components. The parameterization schemes are tested by comparing the area-averaged fluxes from the mesoscale model domain (i.e., a hypothetical GCM grid box) to those calculated from the proposed 1D parameterizations. The mesoscale model is thus used as a vehicle to produce a dense ''observation'' network and the results are not sensitive to the model itself. Any decent mesoscale model would have produced similar quasi-observations.

### *Model description*

The model used in the study is a 2D hydrostatic mesoscale model in $\sigma$ coordinates. Its dynamics has been developed originally by Alpert et al. (1982). The model has been further developed, improved, and tested for many types of mesoscale flows (e.g., Alestalo and Savijärvi 1985; Neumann and Savijärvi 1986). Savijärvi (1991) validated the model against an extensive boundary layer dataset for both convective and stable conditions. It has also been used for studies of mesoscale circulations for Mars (Savijärvi and Siili 1993), with validation against the Viking lander observations.

The model equations are given in Alpert et al. (1982) and in Alestalo and Savijärvi (1985). In short, its parameterizations are the following: Monin–Obukhov surface layer, stability- and wind shear–dependent vertical diffusion, radiation as in the High Resolution Limited Area Model (Savijärvi 1990), removal of supersaturation into clouds, horizontal diffusion by a weak implicit filter, one-layer energy balance snow algorithm, and snow-free soil parameterization similar to Noilhan and Planton (1989).

The model version used has 130 horizontal and 30 vertical grid points. The two lowest atmospheric levels are at about 3.5 m and 10 m and the domain top is at about 3.2 km. Horizontal grid intervals are 4 km for all the experiments, except for the cases of small-scale heterogeneity. Those were simulated with 400-m horizontal grid length.

If not stated otherwise, in our experiments the initial $u$, $v$, $T$, and $q$ profiles are given as an Ekman–Taylor

spiral, 0.0065 K $m^{-1}$ lapse rate, and 50% relative humidity, respectively. Initial time for all of our simulations is 0500 LST.

## 3. Parameterization of turbulent fluxes

### *a. Large-scale heterogeneity (typically >10 km)*

At large scales of heterogeneity, it may be valid to divide the grid area into subareas; this approach is often called the mosaic approach. However, if there is a strong variability in the boundary layer characteristics, the use of spatially homogeneous atmospheric conditions at the reference level may cause the mosaic method to fail to predict the area-averaged turbulent fluxes. We tested two methods that extend the mosaic approach to incorporate local estimates for the reference level wind speed, air temperature, and specific humidity.

Surface fluxes (stress $\tau$, sensible heat flux $H$, and evaporation $E$) are generally formulated in atmospheric models as

$$\tau = \rho C_D V_z^2, \tag{3}$$

$$H = \rho c_p C_H V_z(\theta_s - \theta_z), \tag{4}$$

$$E = \rho C_E V_z(q_s - q_z), \tag{5}$$

where $V_z$ is the wind speed, $\theta_z$ is the potential temperature, $q_z$ is the specific humidity at the lowest model level, and $\theta_s$ and $q_s$ are the corresponding variables at the surface.

The bulk transfer coefficients are expressed as

$$C_D = \frac{k^2}{\left[\ln\left(\frac{z}{z_{0M}}\right) - \psi_M\left(\frac{z}{L}\right)\right]^2}, \quad \text{and} \tag{6}$$

$$C_H = \frac{k^2}{\left[\ln\left(\frac{z}{z_{0M}}\right) - \psi_M\left(\frac{z}{L}\right)\right]\left[\ln\left(\frac{z}{z_{0H}}\right) - \psi_H\left(\frac{z}{L}\right)\right]}, \tag{7}$$

where $k$ is the von Kármán constant; $z_{0M}$ and $z_{0H}$ are the roughness lengths for momentum and heat, respectively; $\psi_M$ and $\psi_H$ are the stability correction functions for logarithmic profiles; and $L$ is the Obukhov length (e.g., Paulson 1970). Usually it is assumed that $C_H = C_E$. In other words the roughnesses for heat and moisture are taken to be equal. However, for most of the surfaces, the thermal roughness length is smaller than that for momentum, because momentum and heat transfer are determined by different processes. Several numerical values for $z_{0M}/z_{0H}$, the roughness ratio, have been suggested; as an example, a ratio of about 10 has been suggested by Brutsaert (1982), whereas Mahrt and Ek (1993) found that the heat roughness length is about three orders of magnitude smaller than that for momentum, by analyzing aircraft data for scale of order 10 km. Boundary layer simulations performed by Holtslag and Ek (1996) indicated that the choice of Mahrt and Ek (1993) produced closest agreement with measured boundary layer quantities for pine forest in Hydrological Atmospheric Pilot Experiment–Modélisation du Bilan Hydrique. In all of the model simulations, reported herein, the choice of 2 for the roughness ratio was taken. This value recognizes the difference between dominant processes for momentum and heat transfer, although it is arguably small if compared to some suggestions in literature. However, in this study parameterization methods for realistic cases of heterogeneous surfaces and boundary layer structure are developed and tested. Therefore, while it will be interesting to explore sensitivity studies to the roughness ratio, the relative validity of the methods to be compared is not likely to be affected.

Formulations of the surface fluxes and the bulk transfer coefficients depend on the height of the reference level $z$ for the atmospheric variables, $V_z$, $\theta_z$, and $q_z$. If within a GCM grid there is a strong contrast of surface types, say land and sea, boundary layer development for each surface type is very different as well and there are internal boundary layers. In turn, true atmospheric variables at the level corresponding to the lowest level of the GCM may be very inhomogeneous. However, the basic mosaic method assumes area-averaged values. In our study, two extensions to the basic mosaic method to incorporate spatial variability in air temperature, wind speed, and specific humidity at the reference level, were considered.

The definition for the blending height proposed by Mason (1988) assumes that the flow is at that particular level both independent of the horizontal position and still in equilibrium with the underlying local surface. Of course, these two conditions cannot be strictly met at the same height and blending height should be considered as an approximate scale height. In other words, above that height the areally averaged mean flow profiles over heterogeneous surfaces are assumed to follow logarithmic profiles with the effective roughness lengths that represent the mixture of surfaces, below this level the flow profiles for each surface type assume logarithmic profiles with the local roughnesses.

If the GCM reference level is below the blending height, atmospheric variables vary spatially in the basic mosaic method. This case is typical for large-scale heterogeneity (>10 km). The opposite case, in which the blending height is located below the reference level, is addressed in the next section. In a practical example, if the lowest model level is at 50 m and the patch size is 20 km, a rough estimate for the blending height is 100 m (Mason 1988). In that case the wind speed, air temperature, and specific humidity vary at the reference level and the basic mosaic method may not be valid. If, on the other hand, the patch size is 5 km, the blending height is at about 25 m and the lowest model level is above it.

The typical GCM lowest level is at 25–100 m—for example, the lowest level of the European Centre for

Medium-Range Weather Forecasts model is at about 30 m. Therefore the reference level used to calculate the fluxes in all of the surface flux parameterizations, which were considered in our study, was about 26 m, which is the third lowest sigma level of the mesoscale model.

The first method to be applied to extend the basic mosaic method, is modified from an approach proposed by Vihma (1995). It uses stability-corrected logarithmic profiles to calculate local wind speed, air temperature, and specific humidity estimates at the reference level over each patch instead of a common value. Briefly, the method proceeds with the following steps.

Step 1: The friction velocity $u_*$, temperature scale $\theta_*$, and humidity scale $q_*$, are computed for each patch using Monin–Obukhov theory applied at the common blending height, $l_b$:

$$u_*^i = \frac{\langle U_{l_b}\rangle k}{\left[\ln\left(\frac{l_b}{z_{0M}^i}\right) - \psi_M\left(\frac{l_b}{L^i}\right)\right]}, \tag{8}$$

$$\theta_*^i = \frac{(\langle\theta_{l_b}\rangle - \theta_s^i)k}{\left[\ln\left(\frac{l_b}{z_{0H}^i}\right) - \psi_H\left(\frac{l_b}{L^i}\right)\right]}, \quad \text{and} \tag{9}$$

$$q_*^i = \frac{(\langle q_{l_b}\rangle - q_s^i)k}{\left[\ln\left(\frac{l_b}{z_{0H}^i}\right) - \psi_H\left(\frac{l_b}{L^i}\right)\right]}, \tag{10}$$

where $i$ refers to each of the surface type.

Of course, the GCM does not usually predict atmospheric conditions exactly at the blending height. For this reason, the closest level below the estimated blending height was chosen, in order to satisfy the equilibrium requirement. The blending height was the one proposed by Mason (1988) rather than the one by Claussen (1990), which is typically an order of magnitude larger, because local equilibrium is required for the application of the stability-corrected profiles. Instead of the Obukhov length, the bulk Richardson number is used (Launiainen 1995) in order to avoid iterative procedure.

Step 2: The local wind speed, air temperature, and specific humidity are calculated for each surface type at the GCM reference level, $z$, where the transfer coefficients are calculated as well:

$$U_z^i = \frac{u_*^i}{k}\left[\ln\left(\frac{z}{z_{0M}^i}\right) - \psi_M\left(\frac{z}{L^i}\right)\right], \tag{11}$$

$$\theta_z^i = \theta_s^i + \frac{\theta_*^i}{k}\left[\ln\left(\frac{z}{z_{0H}^i}\right) - \psi_H\left(\frac{z}{L^i}\right)\right], \quad \text{and} \tag{12}$$

$$q_z^i = q_s^i + \frac{q_*^i}{k}\left[\ln\left(\frac{z}{z_{0H}^i}\right) - \psi_H\left(\frac{z}{L^i}\right)\right]. \tag{13}$$

Step 3: Strict application of these estimates for wind speed, air temperature, and specific humidity would mean that they adjust immediately to the changing terrain. The effects of fetch and height can be accounted for by taking a weighted average of the local estimates and the grid-averaged values:

$$U_z^{i,\text{new}} = g_U U_z^i + (1 - g_U)\langle U_z\rangle, \tag{14}$$

$$\theta_z^{i,\text{new}} = g_\theta \theta_z^i + (1 - g_\theta)\langle\theta_z\rangle, \tag{15}$$

$$q_z^{i,\text{new}} = g_q q_z^i + (1 - g_q)\langle q_z\rangle, \tag{16}$$

where each of the weights $g$ is between zero and one.

Step 4: The surface fluxes are calculated with these new local wind speeds, air temperatures, and specific humidities for each patch of the mosaic and then summed up to the total as in (2).

To some extent the optimal weights, $g_U$, $g_\theta$, and $g_q$ depend on the case of heterogeneity. It was not attempted at this stage to estimate any functional form that would give the (optimal case) dependent weights. Rather, a simple form is suggested that was used in the following simulations. It turned out to give reasonable results for several cases of heterogeneous surfaces. The same weight, $g$, for $g_U$, $g_\theta$, and $g_q$ was used:

$$g = 0.1\left[1 + \ln\left(\frac{z_{0M_{\text{rough}}}}{z_{0M_{\text{smooth}}}}\right)\right], \tag{17}$$

where $z_{0M_{\text{rough}}}$ and $z_{0M_{\text{smooth}}}$ refer to the maximum and minimum roughness lengths within the mosaic elements, respectively.

By definition, the blending height is assumed to exist within the surface layer and it can be argued that it may be too large in some cases for the surface layer formulations to be still valid. However, it was demonstrated by Claussen (1995) that the validity of the blending height as a reference level for surface flux calculations is not very sensitive to this assumption. Moreover, our goal is to find better local estimates for wind speed, air temperature, and specific humidity, while the reference level for surface flux calculations is at 26 m.

Various scales of heterogeneity were simulated to test the methods in more detail under two types of conditions: juxtaposition of wet and dry land surfaces, and a patchy snow cover. Moisture contrast can be particularly strong due to the agricultural land use in arid regions in the summer. In the spring patchy snow cover can persist for relatively long periods, especially when there is a contrast of forest versus clearings within an area of GCM grid. Clearings stay snow covered after the forest canopy is snow free. Usually some snow remains under the canopy, however it typically has only a small effect on energy balance of the forested area and thus on its interaction with the atmosphere (Segal et al. 1991).

The extended mosaic method was first studied for alternating wet and dry surface patches. A summary of the mesoscale model parameters and land surface characteristics are given in Tables 1 and 2. Several values for synoptic scale wind and patch size were considered.

Figure 1 shows the results for a geostrophic wind

TABLE 1. Model parameters for the case of alternating wet and dry surfaces.

| Condition | Value |
|---|---|
| Latitude | 55°N |
| Day of the year | 22 Jun |
| Initialization time | 0500 LST |
| Potential temperature lapse rate | 0.0036 K $m^{-1}$ |
| Initial surface temperature | 283.15 K |

speed of 7 m $s^{-1}$ and patch size of 80 km. The surface sensible heat flux predicted by the basic mosaic method and extended mosaic method are compared to the grid area average fluxes, which represent the ''truth'' and are simply the average fluxes summed over the entire mesoscale model domain. Fluxes calculated by the basic mosaic method are based on area-averaged atmospheric conditions and averaged surface conditions for each patch. The area average heat fluxes were calculated at the same level at which the parameterizations were applied in order to isolate only the effects of the boundary layer heterogeneity. Differences in the latent heat and momentum fluxes were relatively small and are not shown here.

The results show that the basic mosaic method predicts slightly higher fluxes as compared to the area-averaged flux, which is true for daytime sensible heat flux in particular. This is consistent with the results of Doran and Zhong (1995).

The use of the stability-corrected profiles generally improved the results, where the blending height differs from case to case. It was found, in particular, that dependence of the blending height on stability is crucial. When the stability is taken into account on the blending height, the vertical distance over which the correction is made, decreases as stability increases. Thus the parameterized nocturnal fluxes are predicted fairly accurately as well, as seen in Fig. 1. The maximum estimated blending height, occurring when the surface layer is most unstable, was 415 m for these simulations.

Next the same method was tested for a case of alternating forest and snow-covered clearing. The model input parameters and surface characteristics are listed in Tables 3 and 4. Although the soil moisture might be unrealistically low for the forested part of the domain, it is useful to test the methods for extreme conditions. Moreover, the evapotranspiration over the forest is limited by various factors and under these particular conditions it is limited mainly by the air temperature, so the evapotranspiration is almost equally low if the the soil was saturated. Now the time of the year and surface type, and in turn the boundary layer development, are quite different from the previous case.

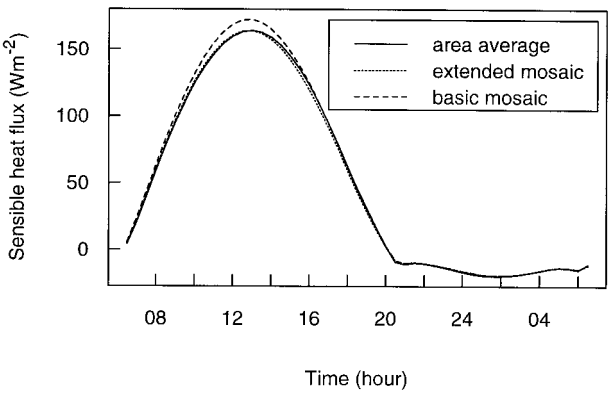


FIG. 1. Sensible heat flux predicted by: basic mosaic method, extended mosaic method, and area-averaged fluxes for alternating wet and dry surfaces. Patch size = 80 km and $U$ = 7 m $s^{-1}$. Maximum blending height is 415 m.

Figure 2 shows model simulations for a geostrophic wind speed of 7 m $s^{-1}$ and patch size of 80 km. The GCM-grid sensible and latent heat fluxes predicted by the basic mosaic method and the extended mosaic method are again compared to the model area average fluxes. Now the differences in the sensible heat flux predictions are larger. Latent heat fluxes are generally small, because there is not much evaporation over the snow cover or over the forest at this time of the year.

Table 5 shows the sensitivity of the basic mosaic method, when either the patch size or the background wind is varied in the patchy snow cover case. It can be seen that if the background wind is increased or the patch size is decreased, differences between the area average sensible heat flux and the basic mosaic method decrease.

A second method, which extends the mosaic method to take into account the boundary layer variability in a simple fashion, was explored. This same approach to extend the basic mosaic method was used also by Seth et al. (1994). The approach is simple and is not very case dependent. In it the features of the mosaic method itself—that is, the variable surface characteristics—are utilized. Also, only air temperature variations are parameterized at this stage. The basic assumption is that

TABLE 2. Surface characteristics for the case of alternating wet and dry surfaces.

| Characteristic | Wet soil | Dry soil |
|---|---|---|
| Albedo | 0.1 | 0.1 |
| Roughness | 0.1 m | 0.1 m |
| Soil moisture content | 0.45 | 0.1 |
| Saturation moisture content | 0.45 | 0.45 |
| Wilting point | 0.15 | 0.15 |

TABLE 3. Model parameters for the case of patchy snow cover.

| Condition | Value |
|---|---|
| Latitude | 55°N |
| Day of the year | 1 May |
| Initialization time | 0500 LST |
| Potential temperature lapse rate | 0.0036 K $m^{-1}$ |
| Initial surface temperature | 273.15 K |

TABLE 4. Surface characteristics for the case of patchy snow cover.

| Characteristic | Forest | Snow-covered clearing |
|---|---|---|
| Albedo | 0.1 | 0.5 |
| Roughness | 0.5 m | 0.01 m |
| Soil moisture content | 0.1 | 0.1 |
| Saturation moisture content | 0.45 | 0.45 |
| Wilting point | 0.15 | 0.15 |

TABLE 5. Midday sensible heat flux predicted by the basic mosaic method vs the area-averaged flux for the case of patchy snow cover as a function of the patch size and the background wind.

| Patch size (km) | Wind ($m\ s^{-1}$) | Basic mosaic ($W\ m^{-2}$) | Area average ($W\ m^{-2}$) |
|---|---|---|---|
| 60 | 5 | 275.6 | 185.4 |
| 60 | 10 | 248.9 | 187.0 |
| 100 | 5 | 353.0 | 178.2 |
| 100 | 10 | 273.3 | 194.2 |
| 80 | 7 | 267.5 | 177.1 |

the surface temperature variation between the surface patches is correlated with the air temperature variations at the reference level. If this assumption is valid, then different roughnesses and patch sizes are absorbed in the method, and only the surface temperature information is needed. This approach depends only on the reference level, so it has to be tuned for the reference level used in any particular GCM. Regressions between the surface temperature differences and the local air temperature differences were found by carrying out mesoscale model simulations for several cases of patch size and geostrophic wind, for alternating wet and dry surfaces. Mean air temperature differences at 26 m (between the surface types) and the corresponding surface temperature differences were calculated and regression coefficient $a$ for the relation $\theta_{z_{\text{patch}}} - \theta_{z_{\text{grid}}} = a(\theta_{s_{\text{patch}}} - \theta_{s_{\text{grid}}})$ was estimated. Here $\theta_z$ and $\theta_s$ are (the mesoscale model's) air and surface temperatures, respectively, and *patch* refers to each of the surface types, *grid* to grid-averaged values.

The regression analysis resulted in the following parameterization for the 26-m reference height:

$$\theta_{z_{\text{patch}}} = \theta_{z_{\text{grid}}} + 0.33(\theta_{s_{\text{patch}}} - \theta_{s_{\text{grid}}}). \qquad (18)$$

The correlation coefficient for this regression equation was 0.98. The data used to derive this relationship were rather limited, so it is important to test the method with an independent case. Figure 3 now shows the re-

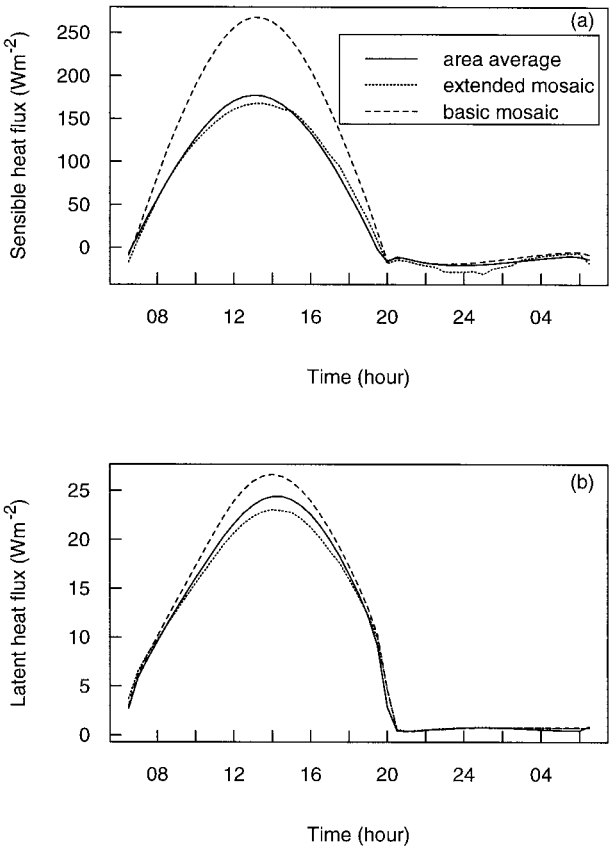


FIG. 2. Sensible (a) and latent heat flux (b) predicted by: basic mosaic method, extended mosaic method, and area-averaged fluxes for patchy snow cover. Patch size = 80 km and $U = 7\ m\ s^{-1}$.

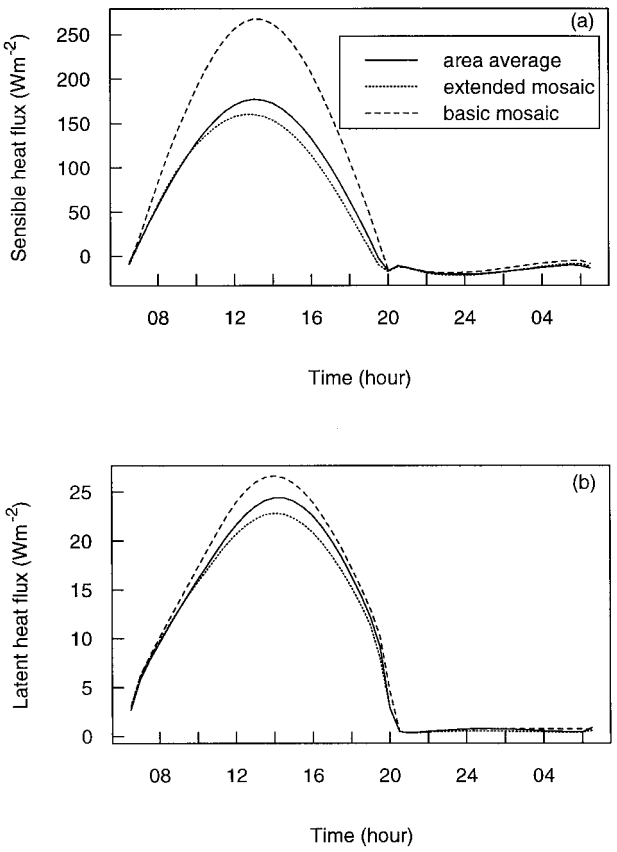


FIG. 3. Same as Fig. 2 except that the extended mosaic method uses the temperature adjustment of Eq. (18).

sults for the same case shown in Fig. 2, but now the extended mosaic method takes into account the variability in the atmospheric variables at the reference level only through the temperature adjustment shown above. This is an independent case to test the parameterization (18), with roughnesses, albedos, etc., quite different to those used to establish the correlation relationship. It can be seen that the temperature adjustment clearly improves the sensible heat flux predictions, but it is not as good as the extended mosaic method, which calculated local values also for the wind speed and specific humidity at the reference level. However, the proposed approach to adjust the temperature through simple correlation relationship is computationally fast and easy to implement in any mosaic approach. For the latent heat flux the differences between the area average flux and the basic mosaic are quite small and the extended mosaic underestimates the fluxes. Generally the differences in the latent heat fluxes are small and it can be concluded that usually the basic mosaic method at large scale is able to predict the latent heat and momentum fluxes reasonably, but in the cases of strong surface heterogeneity the extended mosaic method can improve the surface sensible heat flux predictions. It is also emphasized that for the weight, $g$, a simple form was used. It is likely that the method can be further improved, if a functional relationship between the weight and the case-dependent parameters, such as background wind, patch size, and roughness length, is estimated.

### b. Small-scale heterogeneity (typically <10 km)

If the blending height is above the reference level, then the flow properties, and thus the time averaged flux at that level, vary spatially. This type of problem was addressed in the previous section. If, on the other hand, the scale of heterogeneity is not large enough that the blending height would extend up to the reference level, flow at the reference level is not in equilibrium with the local surfaces. At this small scale, the basic mosaic method may not be strictly applicable (Mahrt 1996). One possibility to model this scale was proposed by Blyth (1995). She addressed the problem mainly theoretically, so a strict test of the approach is still needed. The method presented herein borrows from the three-resistance theory of Blyth (1995), but several assumptions are invoked to modify the method for operational flexibility. This method is also an extension to the basic mosaic method, because the basic mosaic method does not incorporate horizontal advection effects between the surface patches, whereas the extension proposed by Blyth (1995) accounts for these effects.

The proposed method basically distinguishes the properties of the flow above and below the blending height: above the blending height the areally averaged mean flow profiles over heterogeneous surfaces are assumed to follow logarithmic profiles with effective roughness lengths and below it the flow profiles assume logarithmic profiles with each local surface type (i.e., local roughness lengths). The approach can be summarized as follows.

Step 1: Wind speed, air temperature, and specific humidity at the GCM reference level, $z$, located above the blending height, are used together with the overall friction velocity, temperature scale, and humidity scale to calculate wind speed, air temperature, and specific humidity at the blending height. In this sense the method is similar to that of Vihma (1995), except that now overall conditions are used to find $u_*$, $\theta_*$, and $q_*$, as opposed to the surface properties of each patch in the mosaic method. In the following, in the absence of calibration, a very simple way to find these effective parameters was assumed. The effective roughnesses for heat and momentum were weighted logarithmic averages of the values assigned for each land cover type; for both (heat and momentum) roughness lengths a weight of 0.5 was assumed:

$$u_* = \frac{\langle U_z \rangle k}{\left[\ln\left(\frac{z}{z_{0M}}\right) - \psi_M\left(\frac{z}{L}\right)\right]}, \tag{19}$$

$$\theta_* = \frac{(\langle \theta_z \rangle - \theta_s)k}{\left[\ln\left(\frac{z}{z_{0H}}\right) - \psi_H\left(\frac{z}{L}\right)\right]}, \quad \text{and} \tag{20}$$

$$q_* = \frac{(\langle q_z \rangle - q_s)k}{\left[\ln\left(\frac{z}{z_{0H}}\right) - \psi_H\left(\frac{z}{L}\right)\right]}. \tag{21}$$

Step 2: The wind speed, air temperature, and specific humidity are calculated at the blending height, $l_b$:

$$U_{l_b} = \frac{u_*}{k}\left[\ln\left(\frac{l_b}{z_{0M}}\right) - \psi_M\left(\frac{l_b}{L}\right)\right], \tag{22}$$

$$\theta_{l_b} = \theta_s + \frac{\theta_*}{k}\left[\ln\left(\frac{l_b}{z_{0H}}\right) - \psi_H\left(\frac{l_b}{L}\right)\right], \quad \text{and} \tag{23}$$

$$q_{l_b} = q_s + \frac{q_*}{k}\left[\ln\left(\frac{l_b}{z_{0H}}\right) - \psi_H\left(\frac{l_b}{L}\right)\right]. \tag{24}$$

Step 3: The surface fluxes, separately for all patches, are calculated at the blending height. The larger is the vertical distance between the reference level and the blending height below it, the larger are the advection effects.

A complication now appears: when the parameterization methods at the larger scale of heterogeneity were compared in the previous section, the boundary layer variability extended well above 26 m, the level used throughout this study to represent the GCM-reference level and thus the level used by the parameterization methods. In that case, by calculating the ''truth'' at that same level, the only difference between the truth and

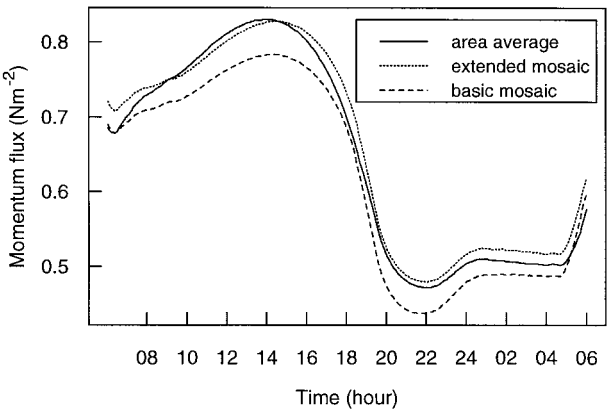


FIG. 4. Momentum flux predicted by: mosaic method, extended mosaic method [further modified from Blyth (1995)] and area-averaged flux for patchy snow cover. Patch size = 2 km and $U$ = 20 m s$^{-1}$.

the fluxes predicted by the proposed parameterizations was whether the boundary layer variability was taken into account or not. Therefore the differences could be explained by the effects of boundary layer variability.

Now the blending height is below the GCM reference level and the main source for different predictions is the horizontal advection effect, which is ''felt'' at the lower levels. In other words, although 26 m is used to test the parameterization methods, a lower level is required for the calculation of the grid area average flux (which represents the truth), if we want to isolate these effects. However, by using a lower reference level for the grid area-averaged flux (predicted by the mesoscale model), another potential effect is introduced; now the fluxes depend to some extent also on the height of the reference level. Of course, if the constant-flux layer assumption was strictly valid, this height dependency would not be present. However, above the first mesoscale model level the turbulence is described by K theory, which cannot strictly support the constant-flux layer assumption. Therefore some height dependency, for both the homogeneous and heterogeneous conditions, is inherent. For this reason, the truth represented in Fig. 4 was chosen so that only small differences in the predicted fluxes for the homogeneous case occurred if they were calculated at 26 m or at the level chosen for truth. This requirement resulted in choosing the second lowest sigma level of the mesoscale model (at 10 m) for the calculations of area-averaged fluxes.

For several cases of the geostrophic wind, the patch size, and the type of surface discontinuity, it was found that in the surface sensible and latent heat fluxes the horizontal advection effects are relatively small, but they are now relatively large for the momentum fluxes. This is opposite to what was found in the larger scale of inhomogeneity in the previous section. Figure 4 shows the results for the momentum flux predictions for the case of alternating forest and snow cover (which induced the largest differences between the basic mosaic method and the area average flux). The mesoscale model parameters and surface characteristics are the same as in the previous case for the larger scale of heterogeneity and are shown in Tables 3 and 4. Again, the fluxes are predicted by the basic mosaic method and the extended mosaic method, described above, and are compared to the area-averaged momentum flux. In the case shown in Fig. 4 the geostrophic wind speed is 20 m s$^{-1}$ and the patch size is 2 km only. The mesoscale model grid length is 0.4 km.

It is apparent that the advection effects are relatively small. However, the use of the blending height to calculate the fluxes is able to capture most of these minor differences. Further simulations (not shown) indicated that when either the geostrophic wind speed decreases or the patch size increases, the differences between the simulations further decrease. Of course, if the scale increases enough, the effects of the boundary layer heterogeneity, which were investigated in the previous section, start to dominate. It can be argued that if there are only minor advection effects for patchy snow cover, when the scale of heterogeneity is 2 km or more, conditions for stronger differences do not usually persist.

The total momentum transfer consists of skin drag and form drag, according to the drag-partition theory (Arya 1975). The form drag is due to the drag from the obstacles. From the point of view of the 1D parameterization methods, the form drag introduces an additional mechanism for the surface–atmosphere momentum exchange, which has to be incorporated. It is likely that an appropriate method to capture the nature of the momentum transfer for heterogeneous surfaces would be through the drag partition theory, as suggested by Klaassen and Claussen (1995) in conjunction with the three-resistance model. The suggested method may be considered as a step into this direction.

## 4. Parameterization of mesoscale fluxes

Organized mesoscale circulation cells—for example, sea breezes—may be generated by landscape discontinuities on scales of 10–200 km (Segal and Arritt 1992). These circulations are occurring at scales smaller than resolved by GCMs. Numerical and analytical studies have shown that in the upper part of the boundary layer the vertical fluxes associated with such thermally driven circulations may exceed the turbulent vertical fluxes (e.g., Seth and Giorgi 1996; Dalu et al. 1996). So far, there have been only very few observational studies due to the lack of comprehensive data. One of them, carried out by Zhong and Doran (1995), was based on the observations from a field experiment over a region characterized by warm, dry sagebrush and grassland steppe and cooler irrigated farmland at scale of 10 km or more. For their study area the mesoscale fluxes were relatively small. Idealized numerical experiments may generate larger fluxes if compared to the real world conditions. Nonetheless, strong landscape contrasts exist also in the

real world (e.g., sea and land contrast, fractional snow cover, etc.) and especially for long low-resolution climate simulations may be beneficial that these unresolvable systematic mesoscale effects are parameterized. Inclusion of mesoscale gravity wave drag has improved both medium-range forecasts and climate simulations.

A general approach to parameterize the thermally driven mesoscale fluxes was suggested by Zeng and Pielke (1995) and Lynn et al. (1995). However, it is attempted here to find somewhat simpler expressions based on linear theory, if possible, extending on Savijärvi's (1995) suggestion. Also, one of the main motivations was to produce parameterizations, which are robust and validated with several types of surface heterogeneities. In both studies mentioned above, a version of the Regional Atmospheric Modeling System (RAMS) developed at Colorado State University was used. The study presented in this paper is an extension to these earlier attempts, but is using an independent mesoscale model. Only the mesoscale sensible and latent heat fluxes were considered as the mesoscale momentum fluxes are arguably small in the thermally driven mesoscale circulations, as shown, for example, in Savijärvi (1995).

### *a. Parameterization*

In this study, in order to establish the parameterizations, we used alternating patches of moist and dry soil surfaces with strip sizes of 60 km, 80 km, and 120 km under background winds of 3 m $s^{-1}$, 6 m $s^{-1}$, and 9 m $s^{-1}$ blowing across the surface discontinuity. The model parameters and land surface characteristics are those given in Tables 1 and 2, except that the latitude is 45° N, the initial surface temperature is 288.15 K, and in addition to the extreme moisture content of 0.45, also the moisture content of 0.2 for the wet surface is considered.

Figure 5 shows an example of the mesoscale and turbulent fluxes for patch size of 120 km and background wind of 3 m $s^{-1}$. The mesoscale sensible heat fluxes are very similar to those simulated by Avissar and Chen (1993), for example. On the other hand, if they are compared to those predicted by Zeng and Pielke (1995), they are smaller. Of course, these simulation studies do not have exactly identical forcings and so cannot be strictly compared. The strength of the simulated mesoscale fluxes depend on the model characteristics, such as the horizontal and vertical resolution and the hydrostatic assumption. For instance, Avissar and Chen (1993) and Zeng and Pielke (1995) used a nonhydrostatic model with horizontal grid elements of 10 km and 2 km, respectively, whereas in our study a hydrostatic model with a horizontal resolution of 4 km was used. Better horizontal resolution and nonhydrostatic model allows stronger vertical motions and mesoscale circulations. In our simulations, the magnitudes of the mesoscale fluxes are comparable to the turbulent fluxes in the upper part of the boundary layer, although

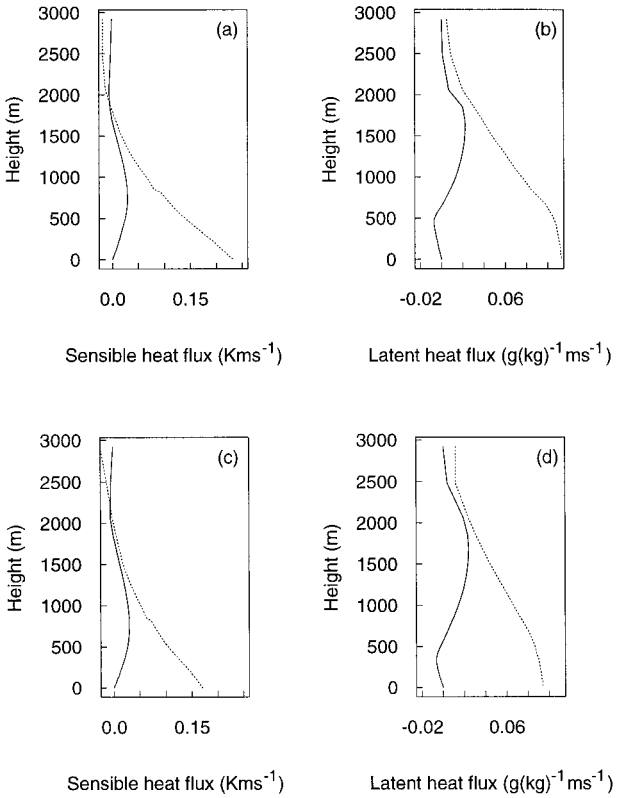


FIG. 5. Vertical profiles of the area-averaged mesoscale (solid line) and turbulent (dashed line) sensible heat fluxes in (a) 1300 LST, (c) 1500 LST; and mesoscale (solid line) and turbulent (dashed line) latent heat fluxes in (b) 1300 LST, (d) 1500 LST. Patch size = 120 km and $U$ = 3 m $s^{-1}$.

in some studies (e.g., in Zeng and Pielke 1995), the mesoscale fluxes relative to the turbulent fluxes have been more significant.

Zeng and Pielke (1995) kept latitude constant and used a 2D version of RAMS, while Lynn et al. (1995) varied latitude and used a 3D RAMS version allowing for more complex surface configurations. In these respects, our study is more like that of Zeng and Pielke (1995), since latitude is kept constant and a 2D model is used. The range of background winds and patch sizes in our experiment is also similar to that of Zeng and Pielke (1995).

In Zeng and Pielke (1995) and Lynn et al. (1995) the robustness of the parameterizations was tested by varying the surface and the atmospheric conditions, but the type of surface heterogeneity was the same—that is, alternating wet and dry surfaces. We argue that it is essential to validate the parameterizations for many types of inhomogeneous surfaces, since many parameters used in these schemes, such as the boundary layer humidity and temperature, may vary considerably from case to case, from sea breeze to snow breeze, for example.

In our study dimensionless mesoscale heat fluxes

were parameterized by using dimensionless parameters. The vertically damped sine wave structure chosen for the mesoscale sensible heat flux profile is taken from Defant's linear sea breeze theory (see Pielke 1984; Savijärvi 1995). For the moisture flux, linear models are not readily available for guidance, hence the quadratic vertical structure in $z$ with four parameters is chosen. It was desired to have as few parameters as possible. We started with key parameters and groups using the Buckingham Pi theory. Based on extensive analysis, the number of groups was reduced. Combining several groups and parameters resulted finally in the following parameterizations for the mesoscale sensible and latent heat fluxes, respectively,

$$\frac{\langle w'\theta'\rangle}{\langle w''\theta''\rangle_{t-2}} = c1\frac{\theta\theta_{s_{t-2}}\Delta\theta_{s_{t-2}}}{T_0^3}\frac{L_s\omega}{c2\dfrac{g}{\omega}+U}\sin\left(\frac{zT_0\omega}{c3\langle w''\theta''\rangle_{t-2}}\right) \times \exp\left(\frac{-zT_0\omega}{c4\langle w''\theta''\rangle_{t-2}}\right), \quad (25)$$

and

$$\frac{\langle w'q'\rangle}{\langle w''q''\rangle} = c1Q\frac{\theta_{s_{t-2}}\Delta\theta_{s_{t-2}}}{T_0^2}\frac{L_s\omega}{U}z' + c2Q\frac{\theta_{s_{t-2}}\Delta\theta_{s_{t-2}}}{T_0^2}\frac{L_s\omega}{U}z'^2 + c3Q\frac{\theta_{s_{t-2}}\Delta\theta_{s_{t-2}}}{T_0^2}\frac{L_s\omega}{U}z'^3 + c4Q\frac{\theta_{s_{t-2}}\Delta\theta_{s_{t-2}}}{T_0^2}\frac{L_s\omega}{U}z'^4, \quad (26)$$

where $\theta$ is potential temperature at any particular level $z$, $\theta_s$ is potential temperature at the surface, and $\Delta\theta_s$ is the driving surface temperature contrast between different surface types. Here $L_s$ is the size of the surface patch, $U$ is the geostrophic wind, $\omega$ is dissipation frequency $[2\pi(0.5\text{ day})^{-1}]$. Here $T_0$ is the melting point, 273.15 K; $Q$ is specific humidity at any level $z$; and $g$ is acceleration due to gravity. If there is no $t$ subscript, a variable at the current time step is used, but $t-2$, for example, indicates that the variable is lagged by 2 h. It was found that the use of lagged variables improved the parameterizations. This is understandable, because the observed maximum thermally driven mesoscale circulation lags the driving surface temperature contrast (or the maximum surface sensible heat flux) typically by 2 h. Vertical location, $z'$, was scaled to dimensionless as well:

$$z' = \frac{z\left(\dfrac{g}{c_p}\right)^{1/2}\left(\dfrac{\Delta\langle\theta\rangle}{\Delta z}\right)^{1/2}g}{\omega\langle\omega''\theta''\rangle_{t-2}}, \quad (27)$$

where $\Delta\langle\theta\rangle/\Delta z$ is the vertical gradient of the large-scale potential temperature above the convective boundary layer, $c_p$ is the specific heat at constant pressure.

TABLE 6. Coefficients for the parameterized mesoscale heat fluxes.

| Coefficient | Sensible heat flux | Latent heat flux |
|---|---|---|
| c1 | 3.8 | $-2.308e^{-7}$ |
| c2 | $1.29e^{-4}$ | $3.062e^{-13}$ |
| c3 | 110 | $-8.882e^{-20}$ |
| c4 | 280 | $7.260e^{-27}$ |

From Table 6 it can be seen that for the mesoscale sensible heat flux and latent heat flux, only four coefficients are required in our scheme. In contrast, the sensible and latent heat flux parameterizations of Zeng and Pielke (1995) require 18 coefficients and those of Lynn et al. (1995) require 15 coefficients, for both. In other words, we are proposing drastically simpler expressions.

The main concern was to include all the most important parameters that govern the mesoscale circulation, in a realistic manner. The conditions, such as larger patch size, weaker background wind, or stronger surface temperature contrast, each separately contributes to the stronger mesoscale flux, and the dimensionless groups are formed so that each parameter has a correct influence. In addition to the parameterization evaluation, described in the following section, the sensitivity of the proposed parameterizations was tested by simply varying one parameter at a time to see if the response is appropriate; for example, larger surface temperature contrast, larger patch size, and weaker background wind tends to generate stronger mesoscale circulations.

It must be emphasized that our parameterizations for the mesoscale heat fluxes are valid within the range of background winds that are used to establish them—that is, division by zero in Eq. (26) is not possible.

In this study the geostrophic wind across the change in the surface type was considered. The mesoscale fluxes are different, if the geostrophic wind blows parallel to the surface discontinuity and even for a strong background wind, large mesoscale fluxes can then be induced. We plan to extend our parameterization to cover these cases as well.

### *b. Parameterization evaluation*

The robustness of the above parameterizations was evaluated by varying the surface and atmospheric conditions for alternating moist and dry land surfaces. Furthermore, as an additional and independent case of heterogeneity, the contrast between snow and snow-free surface was used to check whether the method has potential to predict the mesoscale fluxes for quite different driving conditions.

Thus, a set of the following changes was first made to the ''control case''—that is, to the mesoscale model setup that was used to generate the parameterization constants in Table 6. The simulation time was set to about one month earlier, to 20 May, the roughness was reduced from 0.1 m to 0.05 m, and the moisture of the wetter surface was 0.3. The effects of these changes

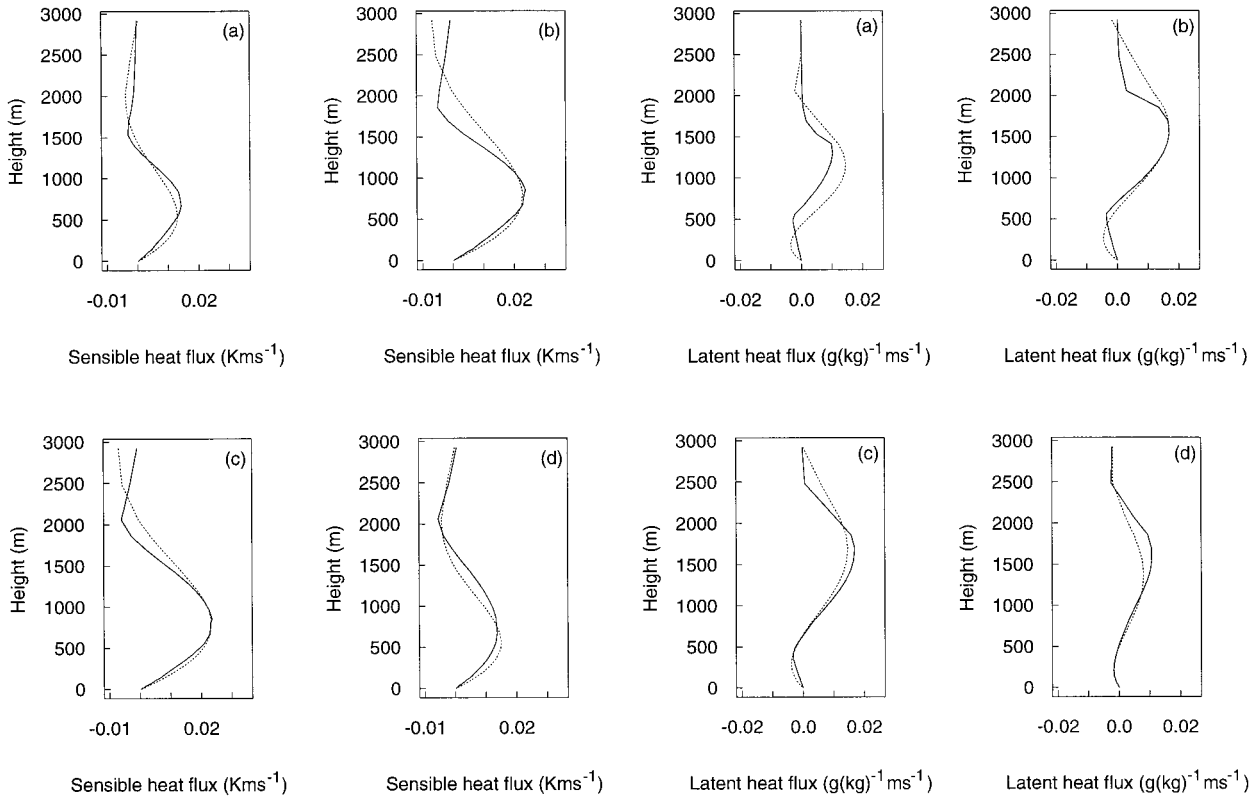


FIG. 6. Vertical profiles of the area-averaged (solid line) and parameterized (dashed line) mesoscale sensible heat flux in (a) 1100 LST, (b) 1300 LST, (c) 1500 LST, and (d) 1700 LST. Patch size = 100 km and $U = 4$ m s$^{-1}$. Initial time is 20 May and roughness is 0.05.

FIG. 7. Vertical profiles of the area-averaged (solid line) and parameterized (dashed line) mesoscale latent heat flux in (a) 1100 LST, (b) 1300 LST, (c) 1500 LST, and (d) 1700 LST. Patch size = 100 km and $U = 4$ m s$^{-1}$. Initial time is 20 May and roughness is 0.05.

were tested for several patch sizes and large-scale winds. The vertical profiles of the mesoscale sensible and latent heat fluxes are shown for one particular case in Figs. 6–7, which are thus independent-sample tests. It is argued that these changes have clear impact on overall conditions affecting the mesoscale fluxes. The roughness reduction by half can strongly affect the surface fluxes and the mean boundary layer characteristics, and in turn, the mesoscale fluxes. Also, the incoming solar radiation is different in 20 May, if compared to the control case, 22 June. Moreover, the soil moisture contrast was different to that in the control case.

Figure 6 shows that the mesoscale sensible heat flux profile is predicted reasonably well by the parameterization. Especially the peak magnitude and its location when the flux is at its strongest (1500 LST) are rather accurate. It can be seen that the sensible heat flux parameterization is quite robust and reproduces the time evolution of the mesoscale flux.

Parameterization for the latent heat flux profile is more problematic (Fig. 7). Although the peak values and locations are again captured quite well, errors early in the day are more pronounced. However, the magnitudes and vertical locations for the peak values are predicted reasonably well. These results are in accordance with those of Zeng and Pielke (1995), who concluded from their statistical parameterization evaluation that the performance of latent heat flux parameterization was not as good as that of sensible heat flux parameterization.

Next, the initial background potential temperature lapse rate was changed from 0.0036 to 0.0058 K m$^{-1}$. Again the vertical profiles of the mesoscale sensible and latent heat fluxes are shown for one particular patch size and wind speed in Figs. 8–9. This change in the stability conditions is slightly stronger than that used by Lynn et al. (1995) to evaluate their parameterization schemes. Latent heat flux predictions have similar deficiencies as in the previous set of simulations, but the errors are somewhat larger. However, these errors are not larger in magnitude than those produced by the schemes suggested by the earlier studies [e.g., see Fig. 13 in Lynn et al. (1995)].

The third set of simulations is the most relevant for the question whether the suggested schemes are general enough to be applicable for many types of heterogeneous surfaces. In this case, the contrast between a snow-covered and snow-free land surface was used. The simulation time was 1 May and initially both snow and the snow-free surface were at the melting point. The

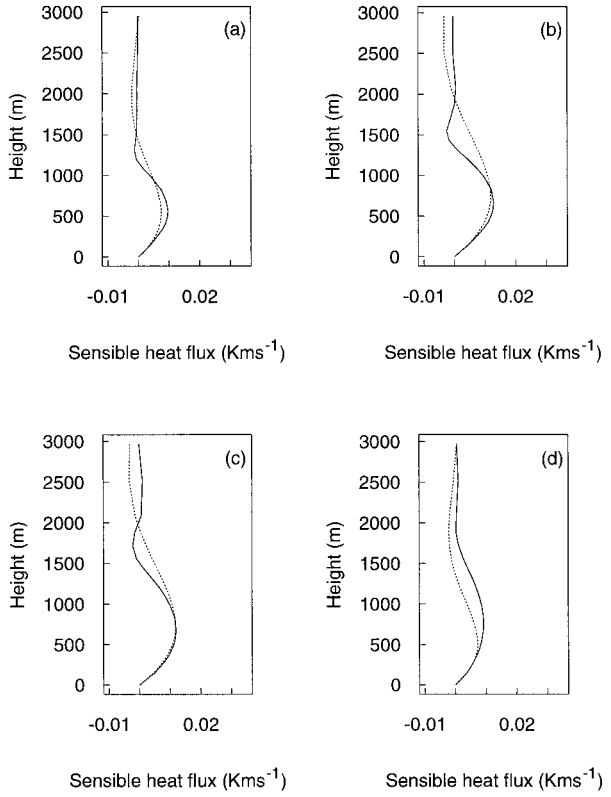


FIG. 8. Vertical profiles of the area-averaged (solid line) and parameterized (dashed line) mesoscale sensible heat flux in (a) 1100 LST, (b) 1300 LST, (c) 1500 LST, and (d) 1700 LST. Patch size = 80 km and $U = 8$ m s$^{-1}$. Initial potential temperature lapse rate 0.0058 K m$^{-1}$.

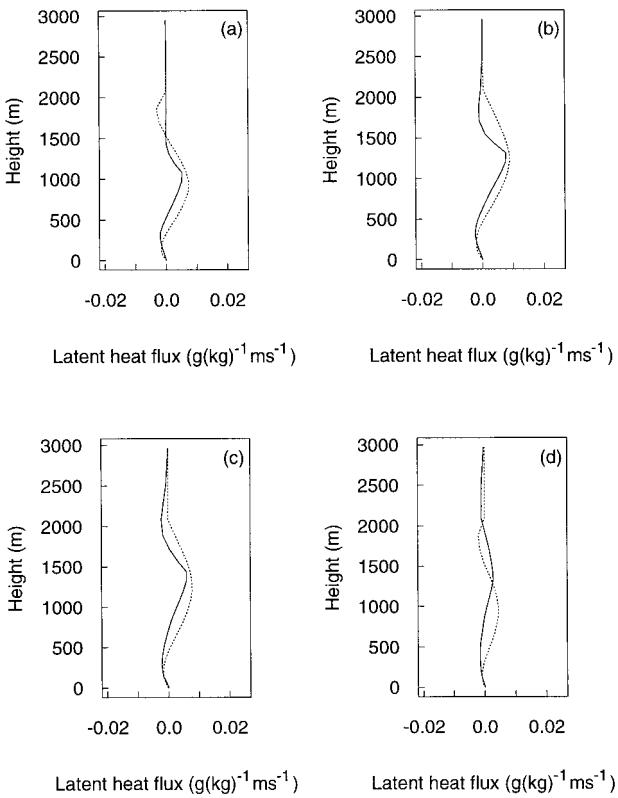


FIG. 9. Vertical profiles of the area-averaged (solid line) and parameterized (dashed line) mesoscale latent heat flux in (a) 1100 LST, (b) 1300 LST, (c) 1500 LST, and (d) 1700 LST. Patch size = 80 km and $U = 8$ m s$^{-1}$. Initial potential temperature lapse rate 0.0058 K m$^{-1}$.

model parameters and land surface characteristics are those given in Tables 3 and 4, except that the latitude is 45° N, and the roughness of the snow-free surface, covered by long grass, is 0.1 m. The soil moisture of the snow-free part of the domain is unrealistically low; however, it is important to validate the parameterization schemes under extreme conditions. The initial surface temperatures are 15 K colder than in the control case, and the overall surface and boundary layer characteristics are quite different if compared to the midsummer wet and dry land surface case. The resulting mesoscale latent heat fluxes are small in these conditions, so only the sensible heat flux profiles are shown (Fig. 10). It can be seen that the parameterization has slightly larger errors than in the earlier cases, but it is still able to capture the main features in these very different surface and boundary layer characteristics.

In addition to the cases described above, the parameterization schemes were tested also for the case of a typical (Baltic Sea) sea breeze circulation and they turned out to be equally robust.

A constant latitude was used in developing the schemes, which is not completely justified (e.g., Savijärvi 1995). An additional set of changes compared to the control case was made: simulations were carried out, in which the latitude was both higher (65°N) and lower (25°N) than 45°N. Figure 11 shows the mesoscale sensible heat fluxes for the latitude of 25°N, which induced the larger differences. The parameterization method is still able to produce the area-averaged fluxes reasonably; however, the errors are somewhat larger than were resulted from the previous changes.

To demonstrate that it is crucial to test the methods for several types of land surface heterogeneity, we tested also the parameterizations of the mesoscale sensible heat fluxes within the boundary layer suggested by Zeng and Pielke (1995) and Lynn et al. (1995) both for the alternating wet-and-dry land surface case and for the patchy snow cover case described above. Figure 12 shows the parameterized mesoscale sensible heat fluxes and the truth for both conditions. The upper panel shows the sensible heat flux, which was induced by a juxtaposition of dry and wet (moisture content of wetter surface is 0.45) surfaces; the model parameters and land surface characteristics are the same as used to generate our parameterizations. The lower panel shows the sensible heat flux generated by the case of the patchy snow cover used above to test the robustness of our parameterization. In both cases the synoptic scale wind speed

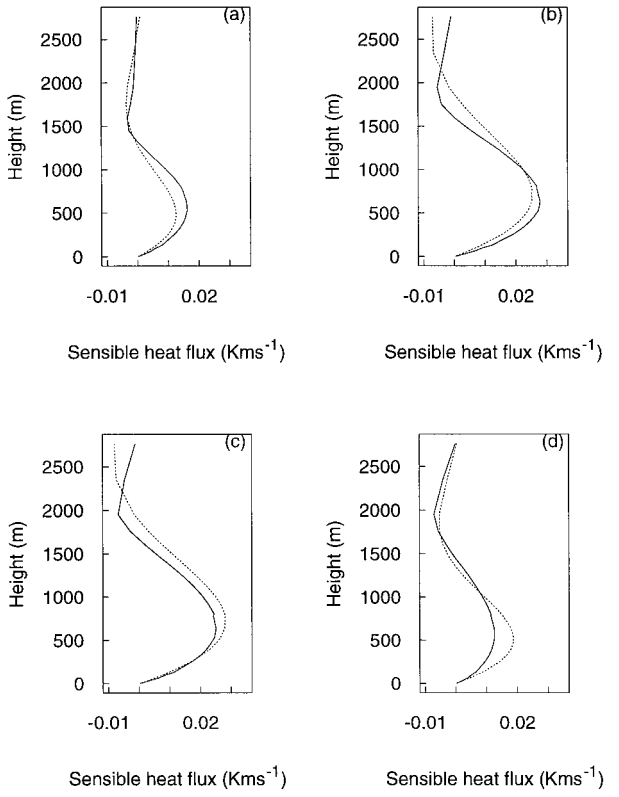


FIG. 10. Vertical profiles of the area-averaged (solid line) and parameterized (dashed line) mesoscale sensible heat flux in (a) 1100 LST, (b) 1300 LST, (c) 1500 LST, and (d) 1700 LST. Patch size = 100 km and $U = 4$ m s$^{-1}$. Initial time is 1 May with fractional snow.

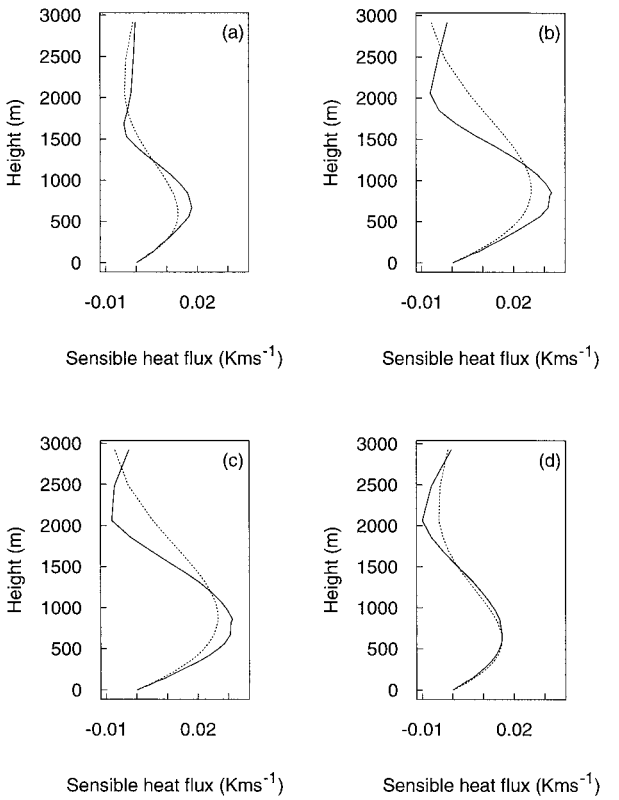


FIG. 11. Vertical profiles of the area-averaged (solid line) and parameterized (dashed line) mesoscale sensible heat flux in (a) 1100 LST, (b) 1300 LST, (c) 1500 LST, and (d) 1700 LST. Patch size = 100 km and $U = 4$ m s$^{-1}$. The latitude is 25°N.

is 4 m s$^{-1}$ and the patch size is 100 km. It can be seen that for the case of the moisture contrast Zeng and Pielke's (1995) parameterization produces a prediction of the mesoscale sensible heat flux that is quite similar to their own simulations (see Fig. 1 of their paper). If the mesoscale sensible heat fluxes predicted by Zeng and Pielke (1995) in Fig. 12a are compared to those produced by our mesoscale model, they are significantly stronger, whereas the mesoscale sensible heat fluxes of Lynn et al. (1995) are quite similar in magnitude to our simulations. The peak fluxes depend on the model characteristics, such as the horizontal and vertical resolution and the hydrostatic assumption.

The lower panel of Fig. 12 shows the mesoscale sensible heat fluxes for the case of patchy snow cover. It is apparent that the method of Zeng and Pielke (1995) has difficulties in predicting the fluxes when the boundary layer characteristics and the surface fluxes are quite different to those that were used to develop their parameterizations. Figure 12 suggests a peak flux of almost 300 W m$^{-2}$ for the snow breeze, which is clearly too strong. Additional analyses show that this large value was caused by the inability of the Zeng and Pielke (1995) scheme to account for the horizontally averaged positive temperature difference between boundary layer top and surface when horizontally averaged surface sensible heat flux is positive (into the atmosphere).

The scheme of Lynn et al. (1995) produces slightly stronger fluxes if compared to the area average flux. This may presumably be attributed to model differences [RAMS was used by Lynn et al. (1995)], whereas their parameterization scheme as such seems to be quite robust in changing conditions.

## 5. Conclusions

Improved parameterization methods for both the surface turbulent and mesoscale fluxes were developed. The performance of the schemes was evaluated by comparing them with the mesoscale model results in many surface configurations and atmospheric conditions. The parameterization of the surface turbulent fluxes was separated into two categories: large-scale heterogeneity and small-scale heterogeneity. This is justified because different effects, to which the GCM parameterization methods should account for, are dominant at different scales. At small scale of heterogeneity the horizontal advection effects near the surface may dominate, whereas at the larger scale of heterogeneity, the parameterizations should incorporate the effects of inhomogeneous at-

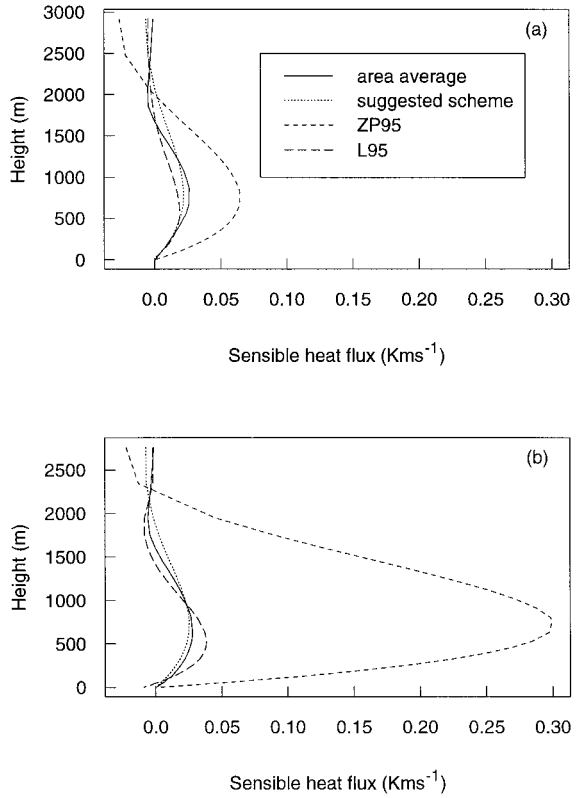


FIG. 12. Vertical profiles of the area-averaged mesoscale sensible heat flux and fluxes parameterized by Zeng and Pielke (1995; ZP95), Lynn et al. (1995) (L95), and the suggested method in 1300 LST generated by alternating wet and dry surfaces (a) and patchy snow cover (b). Patch size = 100 km and $U = 4$ m s$^{-1}$.

mospheric conditions at the lowest GCM model level. When the scale is large enough (and the background wind is weak enough), thermally driven mesoscale circulations may develop. Parameterization methods for these effects—that is, for the mesoscale fluxes—were also developed.

At large scale of heterogeneity it was found that the improvements for the sensible heat flux parameterization, in particular, are needed, whereas the latent heat and momentum fluxes are predicted rather accurately by the basic mosaic method. The extension to the basic mosaic method, modified from Vihma (1995), gave promising results for the larger scales of surface heterogeneity. It could be an important modification to the current GCM schemes, as it is computationally cheap and easy to implement.

Opposite to the large scale, at smaller scales of surface heterogeneity, it was shown that further improvements preferably for the parameterization of momentum transfer are needed. It was demonstrated that these are likely to be carried out by introducing mechanism to incorporate the effects of form drag in conjunction with the three-resistance model proposed by Blyth (1995). A step into this direction was suggested.

For mesoscale heat fluxes simple parameterizations were developed, when compared to the previous work. These turned out to be quite robust.

Finally, all these schemes are based and validated so far on datasets created by a numerical mesoscale model, simply because suitable high-density observations are not available. The methods should be revalidated, when these become available, for instance from the BALTEX observational campaigns.

*Acknowledgments.* I gratefully acknowledge Hannu Savijärvi and Timo Vihma for many discussions and constructive comments on the manuscript. Roni Avissar and Dennis P. Lettenmaier are acknowledged for their comments on an earlier version of the manuscript. This research was supported by the European Union-funded BALTEX project (Newbaltic ENV4-CT95-0072) and by the Nessling Foundation.

## REFERENCES

Alestalo, M., and H. Savijärvi, 1985: Mesoscale circulations in a hydrostatic model: Coastal convergence and orographic lifting. *Tellus,* **37A,** 156–162.

Alpert, P., A. Cohen, E. Doron, and J. Neumann, 1982: A model simulation of the summer circulation from the Eastern Mediterranean past Lake Kinneret in the Jordan Valley. *Mon. Wea. Rev.*, **110,** 994–1006.

Arya, S. P., 1975: A drag partition theory for determining the large scale roughness parameter and wind stress on the Arctic pack ice. *J. Geophys. Res.*, **80,** 3447–3454.

Avissar, R., 1992: Conceptual aspects of a statistical–dynamical approach to represent landscape subgrid-scale heterogeneities in atmospheric models. *J. Geophys. Res.*, **97,** 2729–2742.

——, and R. A. Pielke, 1989: A parameterization of heterogeneous land surfaces for atmospheric numerical models and its impact on regional meteorology. *Mon. Wea. Rev.*, **117,** 2113–2136.

——, and F. Chen, 1993: Development and analysis of prognostic equations for mesoscale kinetic energy and mesoscale (subgrid scale) fluxes for large-scale atmospheric models. *J. Atmos. Sci.*, **50,** 3751–3774.

Blyth, E. M., 1995: Using a simple SVAT scheme to describe the effect of scale on aggregation. *Bound.-Layer Meteor.*, **72,** 267–285.

Brutsaert, W. H., 1982: *Evaporation into the Atmosphere—Theory, History, and Applications.* D. Reidel, 299 pp.

Businger, J. A., J. C. Wyngaard, Y. Izumi, and E. F. Bradley, 1971: Flux-profile relationships in the atmospheric surface layer. *J. Atmos. Sci.*, **28,** 181–189.

Claussen, M., 1990: Area-averaging of surface fluxes in neutrally stratified, horizontally inhomogeneous atmospheric boundary layer. *Atmos. Environ.*, **24A,** 1349–1360.

——, 1995: Flux aggregation at large scales: On the limits of validity of the concept of blending height. *J. Hydrol.*, **166,** 371–382.

Dalu, G. A., R. A. Pielke, M. Baldi, and X. Zeng, 1996: Heat and momentum fluxes induced by thermal inhomogeneities with and without large-scale flow. *J. Atmos. Sci.*, **53,** 3286–3302.

Doran, J. C., and S. Zhong, 1995: Variations in mixed-layer depths arising from inhomogeneous surface conditions. *J. Climate,* **8,** 1965–1973.

Ducoudré, N. I., K. Laval, and A. Perrier, 1993: SECHIBA: A new set of parameterizations of hydrologic exchanges at the land–atmosphere interface within the LMD atmospheric general circulation model. *J. Climate,* **6,** 248–273.

Holtslag, A. A. M., and M. Ek, 1996: Simulation of surface fluxes

and boundary layer development over the pine forest in HAPEX-MOBILHY. *J. Appl. Meteor.,* **35,** 202–213.
Klaassen, W., and M. Claussen, 1995: Landscape variability and surface flux parameterization in climate models. *Agric. For. Meteor.,* **73,** 181–188.
Koster, R. D., and M. J. Suarez, 1992: Modeling the land surface boundary in climate models as a composite of independent vegetation stands. *J. Geophys. Res.,* **97** (D3), 2697–2715.
Launianen, J., 1995: Derivation of the relationship between the Obukhov stability parameter and the bulk Richardson number for flux-profile studies. *Bound.-Layer Meteor.,* **76,** 165–179.
Lynn, B. H., F. Abramapoulos, and R. Avissar, 1995: Using similarity theory to parameterize mesoscale heat fluxes generated by subgrid-scale landscape discontinuities in GCMs. *J. Climate,* **8,** 932–951.
Mahrt, L., 1987: Grid-averaged surface fluxes. *Mon. Wea. Rev.,* **115,** 1550–1560.
——, 1996: The bulk aerodynamic formulation over heterogeneous surfaces. *Bound.-Layer Meteor.,* **78,** 87–119.
——, and M. Ek, 1993: Spatial variability of turbulent fluxes and roughness lengths in HAPEX-MOBILHY. *Bound.-Layer Meteor.,* **65,** 381–400.
Mason, P. J., 1988: The formation of areally averaged roughness lengths. *Quart. J. Roy. Meteor. Soc.,* **114,** 399–420.
Neumann, J., and H. Savijärvi, 1986: The sea breeze on a steep coast. *Contrib. Atmos. Phys.,* **59,** 375–389.
Noilhan, J., and S. Planton, 1989: A simple parameterization of land surface processes for meteorological models. *Mon. Wea. Rev.,* **117,** 536–549.
Paulson, C. A., 1970: The mathematical representation of wind speed and temperature profiles in the unstable atmospheric surface layer. *J. Appl. Meteor.,* **9,** 857–861.
Pielke, R., 1984: *Mesoscale Meteorological Modeling.* Academic Press, 612 pp.
——, G. A. Dalu, J. S. Snook, T. J. Lee, and T. G. E. Kittel, 1991: Nonlinear influence of mesoscale land use on weather and climate. *J. Climate,* **4,** 1053–1069.
Savijärvi, H., 1990: Fast radiation parameterization schemes for mesoscale and short-range forecast models. *J. Appl. Meteor.,* **29,** 437–447.
——, 1991: The United States Great Plains diurnal ABL variation and the nocturnal low-level jet. *Mon. Wea. Rev.,* **119,** 833–840.
——, 1995: Sea breeze effects on large-scale atmospheric flow. *Contrib. Atmos. Phys.,* **68,** 335–344.
——, and T. Siili, 1993: The Martian slope winds and the nocturnal PBL jet. *J. Atmos. Sci.,* **50,** 77–88.
Segal, M., and R. W. Arritt, 1992: Nonclassical mesoscale circulations caused by surface sensible heat-flux gradients. *Bull. Amer. Meteor. Soc.,* **73,** 1593–1604.
——, J. R. Garratt, R. A. Pielke, and Z. Ye, 1991: Scaling and numerical model evaluation of snow-cover effects on the generation and modification of daytime mesoscale circulations. *J. Atmos. Sci.,* **48,** 1024–1042.
Seth, A., and F. Giorgi, 1996: Three-dimensional model study of organized mesoscale circulations induced by vegetation. *J. Geophys. Res.,* **101,** 7371–7391.
——, ——, and R. E. Dickinson, 1994: Simulating fluxes from heterogeneous land surfaces: Explicit subgrid method employing the biosphere–atmosphere transfer scheme (BATS). *J. Geophys. Res.,* **99,** 18 651–18 667.
Vihma, T., 1995: Subgrid parameterization of surface heat and momentum fluxes over polar oceans. *J. Geophys. Res.,* **100,** 22 625–22 646.
Wieringa, J., 1986: Roughness-dependent geographical interpolation of surface wind speed averages. *Quart. J. Roy. Meteor. Soc.,* **112,** 867–889.
Wood, N., and P. J. Mason, 1991: The influence of stability on the effective roughness lengths for momentum and heat flux. *Quart. J. Roy. Meteor. Soc.,* **117,** 1025–1056.
Zeng, X., and R. A. Pielke, 1995: Landscape-induced atmospheric flow and its parameterization in large-scale numerical models. *J. Climate,* **8,** 1156–1177.
Zhong, S., and J. C. Doran, 1995: A modeling study of the effects of inhomogeneous surface fluxes on boundary layer properties. *J. Atmos. Sci.,* **52,** 3129–3142.